A Simple, Minimal Parameter Model for Predicting the Influence of Changing Land Cover on the Land–Atmosphere System[+]

Justin E. Bagley*

Center for Sustainability and the Global Environment (SAGE), and Department of Atmospheric and Oceanic Sciences, University of Wisconsin—Madison, Madison, Wisconsin

Ankur R. Desai

Department of Atmospheric and Oceanic Sciences, University of Wisconsin—Madison, Madison, Wisconsin

Paul C. West

Center for Sustainability and the Global Environment (SAGE), University of Wisconsin—Madison, Madison, Wisconsin, and Institute on the Environment (IonE), University of Minnesota, St. Paul, Minnesota

Jonathan A. Foley

Institute on the Environment (IonE), University of Minnesota, St. Paul, Minnesota

Received 8 December 2010; accepted 31 May 2011

ABSTRACT: The impacts of changing land cover on the soil–vegetation–atmosphere system are numerous. With the fraction of land used for farming and grazing expected to increase, extensive alterations to land cover such as replacing

[+] Supplemental information related to this paper is available at the Journals Online Web site.

* Corresponding author address: Justin E. Bagley, Center for Sustainability and the Global Environment, University of Wisconsin—Madison, 1710 University Ave., Madison, WI 53726.
E-mail address: bagley@wisc.edu

DOI: 10.1175/2011EI394.1

forests with cropland will continue. Therefore, quantifying the impact of global land-cover scenarios on the biosphere is critical. The Predicting Ecosystem Goods and Services Using Scenarios boundary layer (PegBL) model is a new global soil–vegetation–boundary layer model designed to quantify these impacts and act as a complementary tool to computationally expensive general circulation models and large-eddy simulations. PegBL provides high spatial resolution and inexpensive first-order estimates of land-cover change on the surface energy balance and atmospheric boundary layer with limited input requirements. The model uses a climatological-data-driven land surface model that contains only the physics necessary to accurately reproduce observed seasonal cycles of fluxes and state variables for natural and agricultural ecosystems. A bulk boundary layer model was coupled to the land model to estimate the impacts of changing land cover on the lower atmosphere. The model most realistically simulated surface–atmosphere dynamics and impacts of land-cover change at tropical rain forest and northern boreal forest sites. Further, simple indices to measure the potential impact of land-cover change on boundary layer climate were defined and shown to be dependent on boundary layer dynamics and geographically similar to results from previous studies, which highlighted the impacts of land-cover change on the atmosphere in the tropics and boreal forest.

KEYWORDS: Land-use change; Boundary layer; Deforestation; Land–atmosphere interactions; Climate modeling

1. Introduction and motivation

The impact of land-cover change on the environment is well recognized (Foley et al. 2005; Bala et al. 2007; Bonan 1997). To fuel and feed Earth's population, croplands and pastures have expanded to occupy between 30% and 40% of Earth's ice-free land surface, or roughly 5 billion ha, and this conversion is continuing at a rate of 13 million ha yr^{-1} (Ramankutty et al. 2008; see http://faostat.fao.org/). As landscapes change, the goods and services that an ecosystem provides are altered (Costanza et al. 1997; Millennium Ecosystem Assessment 2005; Foley et al. 2005). These goods and services provide basic human needs ranging from food production and water supply to soil formation and waste treatment. The regulation of local and regional climates by land–atmosphere interactions (Foley et al. 2007; West et al. 2010, hereafter WE10) is one of these important services. As natural vegetation is removed and replaced with pastures and croplands, shifts in the surface and atmospheric energy balances occur. These shifts in energy balance alter near-surface climatic state variables such as water vapor and air temperature. However, large uncertainty exists in quantifying the magnitude of regulation geographically.

Land-cover change can influence climate through biogeochemical and biogeophysical pathways (Foley et al. 2003; Meir et al. 2006; Chapin et al. 2008). In this study, we focused exclusively on biogeophysical impacts of land-cover change. Biogeophysical mechanisms directly alter the components of the surface energy balance, surface friction, and the water cycle by altering the physical properties of local vegetation. Plants mediate the exchange of momentum, heat, radiation, and moisture between Earth's surface and the lower atmosphere. By altering land cover, the surface fluxes of radiative, latent (L), sensible (H), and kinetic energy are adjusted. In the case of a tropical forest, the deforestation of a

region to shrubland causes a decrease in surface roughness, a slight increase in albedo, and a strong decrease in L due to the reduction in plant cover (Gash and Nobre 1997; Foley et al. 2003; Anderson et al. 2010). To compensate, H strongly increases in order to conserve the surface energy balance, resulting in an increased boundary layer air temperature. Conversely, in boreal regions, increases in albedo associated with deforestation have been shown to dominate, resulting in lower-atmosphere cooling (Betts 2000; Feddema et al. 2005; Liu et al. 2005; Anderson et al. 2010). Previous studies have suggested that the impact of these surface shifts on global-mean climate is small; however, regional and seasonal impacts can be significant (Bounoua et al. 2002; Feddema et al. 2005).

To date, impacts of biogeophysical effects due to land-cover perturbations have been largely neglected in key simulations of future climate for policy makers, with the focus instead being on biogeochemical impacts (Davin and de Noblet-Ducoudré 2010). Additionally, research into the biogeophysical impacts of large-scale land-cover change has been restricted by reliance on models of intermediate complexity that generally focus on low-resolution millennial-scale simulations (Clausen et al. 2002) or extremely complex numerical models such as general circulation models (GCMs), regional climate models (RCMs), or large-eddy simulations (LESs) (WE10). Although these models are powerful tools, they have inherent drawbacks that make assessing near-surface climate regulation by land-cover change problematic. One restriction of these models is that they are computationally expensive to run and complex to interpret. An implication of this expense is that computational requirements prohibit experiments where large numbers of land-use scenarios are investigated. Although the physics of the land surface and atmosphere in most GCMs, RCMs, and LESs are detailed, this comes at the cost of significantly increasing the number of unknown or crudely estimated parameters that drive the model. Additionally, RCMs and LESs are reliant on transient boundary conditions that can have unforeseen impacts on a simulation. Finally, most GCMs have relatively low vertical resolution near Earth's surface. This makes investigations of near-surface impacts of land use on the atmosphere difficult because of large gradients that characterize transitions between the atmospheric boundary layer (ABL) and free atmosphere (Denning et al. 2008). An alternative approach that addresses these challenges yet adequately represents the atmospheric dynamics is needed to make these modeling approaches more accessible to a broader audience.

The purpose of this study is to present and verify a model designed to test the biogeophysical influence of land-use scenarios on the soil–vegetation–boundary layer system at local, regional, and global scales. Compared to other land surface, boundary layer, or general circulation models, the model we present here contains relatively simplistic physics. Although complexity allows for the simulation of detailed processes, our approach has the advantage of reducing the number of unknown parameters, allowing for easier calibrations of model formulations. Also, our approach is suitable for testing large numbers of land-use scenarios because of massively reduced computational cost. The model was specifically constructed to capture the impact of biogeophysical regulation of climate. This is in contrast to the aforementioned models where the emphasis is on detailed turbulent and radiative structures or on global dynamical flows.

In the following sections, we first describe this new surface energy balance–boundary layer model, then evaluate the model at several comprehensive field

experiments, and finally use the model on a global application in order to answer the following questions:

1) Can we generalize a simple model to accurately simulate the boundary layer state variables across environmental conditions? If so, which biomes and state variables are most realistically simulated? (See sections 2 and 3.)
2) To what extent can mean climatology be used as a base state for modeling perturbations of land-cover change? (See section 3.)
3) How can this model be used to develop simple global indices describing the impact of land-cover change on climate? (See section 4.)
4) What role does boundary layer height adjustment have in modulating the impact of land cover on the atmospheric boundary layer? (See section 4.)

2. Model description

2.1. The PEGASUS land model

To estimate the state of the land surface, we used the Predicting Ecosystem Goods and Services Using Scenarios (PEGASUS) model. Deryng et al. (Deryng et al. 2010) describe the model and emphasize PEGASUS's crop modeling capabilities, where phenology, irrigation, and nutrient application are explicitly simulated. Here, we discuss the model's general attributes and the details of the water/energy balance formulations as these directly influence the surface energy budget and hence the ABL's responses to land-cover change. A comprehensive list of symbols used is in Table 1.

PEGASUS's spatial resolution was the same as its primary input datasets (10′) and had a daily temporal resolution (with the exception of subdaily energy balance and ABL terms, as described below). By default, the PEGASUS model was forced by monthly Climatic Research Unit (CRU) 2.1 30-yr mean values of surface temperature, precipitation, and cloud cover at 10′ latitude/longitude resolution (New et al. 2002). However, comparable datasets from individual years or climate scenarios could be used as input to the model to test impacts of interannual variability. The data from these sets were linearly interpolated to daily values in order to reduce unrealistic step changes. Additionally, a 5′ latitude/longitude resolution map of soil available water capacity regridded to 10′ was used to estimate soil properties (Batjes 2006). Using these inputs, the model estimated key energy, water, and carbon balances of the soil–plant–atmosphere system. However, one implication of the model being forced by climatological data was the implicit assumption that any alterations to Earth's land cover represented relatively small perturbations to the overall climate. This assumption is most likely invalid in scenarios of extreme land-cover conversions such as the deforestation of the entire Amazon rain forest. However, for many realistic scenarios, this supposition should be acceptable, and we explore this further in section 3.

PEGASUS's surface energy balance formulation begins with top of atmosphere estimates of hourly incoming solar radiation, which depend on latitude and orbital parameters as described in Hartmann (Hartmann 1994). These hourly values were compiled to get daily-mean incoming solar radiation SW_{in}. The transmissivity t_r of the atmosphere was calculated using climatological cloud cover C (Friend 1998),

Table 1. List of symbols used in the text and their respective units.

Symbol	Description	Units
Δ	Slope of saturation vapor pressure–temperature curve	Pa K^{-1}
δ_θ	Potential temperature jump at the top of the boundary layer	K
δ_Q	Specific humidity jump at the top of the boundary layer	kg kg^{-1}
ε	Surface emissivity	—
$\varepsilon_{\mathrm{bl,i}}$	Boundary layer emissivity	—
γ_θ	Gradient of potential temperature in the free atmosphere	K m^{-1}
γ_Q	Gradient of specific humidity in the free atmosphere	m^{-1}
γ	Psychometric constant	Pa K^{-1}
λ	Latent heat of vaporization	J kg^{-1}
φ	Sun angle with respect to the zenith	rad
ρ	Air density	kg m^{-3}
θ	Boundary layer potential temperature	K
θ_{index}	Temperature index	K
σ	Stefan–Boltzmann constant	W m^{-2} K^{-4}
dtr_m	CRU 30-yr mean diurnal temperature range	°C
C	Fractional cloud cover	—
E	Actual evapotranspiration	kg m^{-2} s^{-1}
E_c	Canopy evaporation	kg m^{-2} s^{-1}
E_s	Surface evaporation	kg m^{-2} s^{-1}
E_t	Transpiration	kg m^{-2} s^{-1}
f	Coriolis parameter	s^{-1}
G	Surface heat storage	W m^{-2} s^{-1}
H	Surface sensible heat flux	W m^{-2}
H_{top}	Entrainment sensible heat flux	W m^{-2}
LAI	Leaf area index	m^2 m^{-2}
L	Surface latent heat flux	W m^{-2}
L_m	Monin–Obukhov length	m
L_{top}	Entrainment latent heat flux	W m^{-2}
M	Snowpack melt	mm day^{-1}
N	Brunt–Väisälä frequency	s^{-1}
P	Daily-mean precipitation	mm day^{-1}
PE	Potential evapotranspiration	kg m^{-2} s^{-1}
q_{index}	Moisture index	mm H_2O
Q	Boundary layer specific humidity	kg kg^{-1}
R	Snow proportion of precipitation	—
R_n	Net longwave radiation	W m^{-2}
$R_{\mathrm{net},i}$	Full spectrum net radiation	W m^{-2}
$R_{fd,i}$	Downwelling longwave radiation emitted from the free atmosphere	W m^{-2}
$R_{bd,i}$	Downwelling longwave radiation emitted from the boundary layer	W m^{-2}
$R_{bu,i}$	Upwelling longwave radiation emitted from the boundary layer	W m^{-2}
R_{in}	Net daytime radiation	W m^{-2}
$\mathrm{SW}_{\mathrm{in}}$	Daily-mean shortwave radiation incident on surface	W m^{-2}
$\mathrm{SW}_{\mathrm{out}}$	Daily-mean shortwave radiation reflected by surface	W m^{-2}
Δt	Time step length	s
t_r	Atmospheric transmissivity	—
T_m	Daily-mean surface temperature	°C
$T_{s,i}$	Diurnally varying surface temperature	°C
U	Surface wind speed	m s^{-1}
$U*$	Friction velocity	m s^{-1}
z_i	Boundary layer height	m

$$t_r = 0.251 + 0.509(1 - C). \quad (1)$$

The land surface partitions the incoming shortwave radiation as

$$\mathrm{SW_{in}} = \mathrm{SW_{out}} - R_n - L - H - G, \quad (2)$$

where $\mathrm{SW_{out}}$ is linearly dependent on surface albedo, which was calculated as a function of leaf area index, snow cover, vegetative fraction, and literature-derived values (Oke 1987; Eugster et al. 2000; Baldocchi et al. 2008). Here, R_n and G represent the daily-mean net longwave radiation and surface energy storage, respectively. The daily-mean latent heat flux L was determined following a water-balance method described below. Net longwave radiation is dependent on daily-mean surface temperature T_m and cloud cover C (Linacre 1968),

$$R_n = [0.2 + 0.8(1 - C)](107.0 - T_m). \quad (3)$$

On the daily time scale, G was assumed to be zero, which is consistent with other global ecosystem models. Finally, PEGASUS's daily-mean sensible heat flux was calculated using a mass-balance approach by solving for H in Equation (2).

Water balance in PEGASUS was estimated using an approach that is similar to that of the Lund–Potsdam–Jena (LPJ) model (Gerten et al. 2004). It includes processes representing precipitation, canopy and soil evaporation, transpiration, two-layer soil moisture storage, surface runoff, percolation below the root zone, and snow cover (Figure 1).[1] The proportion of precipitation that fell as snow R was determined as a function of T_m using the formula of Legates and Bogart (Legates and Bogart 2009),

$$R = [1 + 1.61(1.35)^{T_m}]^{-1}. \quad (4)$$

The melting of the snowpack M was determined using a degree-day formulation that depends on precipitation P and T_m (Choudhury and Digirolamo 1998),

$$M = (1.5 + 0.007P)T_m. \quad (5)$$

The depth of the two soil moisture layers were 0–50 cm and 50–150 cm, and the moisture contained in these layers was modeled as a function of precipitation or snowmelt, transpiration, root uptake, and percolation. The summation of percolation below the root zone and soil moisture in excess of the available water capacity of the two soil layers was considered to be runoff. Potential evapotranspiration PE was calculated using the Priestley–Taylor equation (Monteith 1995),

$$\mathrm{PE} = \alpha \frac{R_{\mathrm{in}}\Delta}{\lambda(\Delta + \gamma)}, \quad (6)$$

where α is the Priestley–Taylor coefficient, R_{in} is the net supply of energy from radiation, λ is the latent heat of vaporization, and Δ and γ are temperature-dependent

[1] Supplemental files for Figures 1, 2, and 3 are available at the Journals Online Web site: http://dx.doi.org/10.1175/2011EI394.s1.

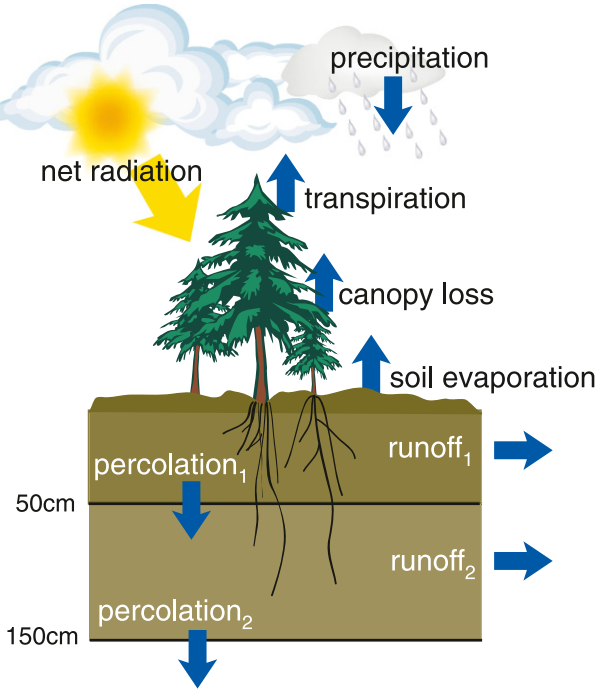

Figure 1. Schematic illustrating the stocks (boxes) and fluxes (arrows) that are components of the water-balance calculations of PEGASUS. Land-cover change affects multiple parameters that modify the fluxes, including fraction of vegetation cover, albedo, maximum rate of transpiration, potential leaf area index, and the rooting profile.

properties of water vapor and moist air. Actual evapotranspiration E was then calculated as

$$E = E_c + E_s + E_t, \tag{7}$$

with E_c being canopy evaporation, which was estimated as a function of precipitation, vegetation cover, and temperature (Prentice et al. 1993). The term E_s is soil evaporation, and E_t is transpiration; both are calculated as functions of air temperature and soil moisture (Campbell and Norman 2000). If E was greater than PE, then E_c, E_s, and E_t were scaled such that E = PE. Once the actual evapotranspiration was calculated, the daily-mean latent heat flux was trivially determined ($L = \lambda E$).

2.2. The bulk boundary layer model

There is a range of boundary layer schemes that have been created in the past few decades. At the complex edge of the spectrum lie LESs that are capable of conducting detailed simulations of much of the turbulent structure of the ABL (Moeng 1984). As more of the turbulence becomes parameterized, the complexity and cost of ABL schemes diminishes exponentially. Taking this reductionist

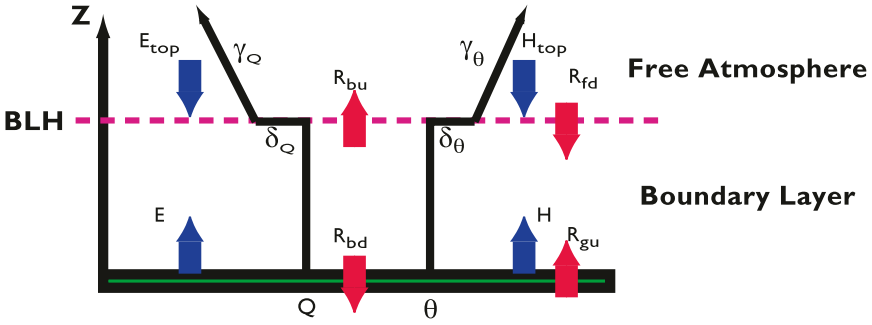

Figure 2. Schematic of bulk boundary layer model. Blue arrows represent sensible and latent heat fluxes into the boundary layer. Red arrows are longwave radiative energy fluxes into and out of the boundary layer. The radiative fluxes are described in more detail within the text (section 2.2.2). The black lines indicate the general profiles of specific humidity Q and potential temperature θ. The term δ designates the discrete jumps of Q and θ at the top of the boundary layer, and γ represents gradients of Q and θ above the boundary layer.

philosophy as far as possible while retaining physical validity produces a cheap model that simulates the ABL as a single layer and only models its bulk properties (Stull 1988). For our purposes of investigating the impact of land-cover change scenarios on the ABL, we were primarily interested in changes to the mean state variables including potential temperature θ, specific humidity Q, and ABL height z_i and not the detailed structure of the ABL itself. This made a bulk model of the ABL ideal for our purposes, though at the cost of losing specificity of atmospheric gradients within the ABL that can influence local stability.

The basic structure of the bulk ABL model is graphically depicted in Figure 2. The ABL model assumed specific humidity and potential temperature to be well mixed throughout the ABL. This is a reasonable assumption for a daytime convective ABL. During the night, surface fluxes of heat and moisture become very small because of the loss of incoming radiant energy and closure of plant stomata. This commonly causes the ABL to become decoupled from the land surface with mesoscale and synoptic atmospheric conditions dominating (Stull 1988; Campbell and Norman 2000). As a result of this decoupling and in the absence of a more robust model of the full atmosphere, we have chosen to focus on modeling the daytime ABL response, with daily relaxation to CRU 30-yr mean climatology. The ABL was initialized to be near the dewpoint at sunup and allowed to respond to diurnal variations in sensible, latent, and radiative energy fluxes as described below.

2.2.1. Diurnally varying latent and surface heat fluxes

The ABL responds to changes in land cover through its influence on the surface energy fluxes as well as changes in surface roughness. This evolution occurs on time scales shorter than the daily time step of the PEGASUS land model (Stull 1988). Additionally, on subdaily time scales the heat storage term in Equation (2) can no longer be assumed to be negligible. To rectify these issues, we began by

Table 2. List of constants used in the text and their respective values.

Constant	Value	Description
α	1.0	Priestley–Taylor coefficient (—)
ε	1.0	Surface emissivity (—)
π	3.141 59	pi (—)
σ	5.6704×10^{-8}	Stefan–Boltzmann constant (W m^{-2} K^{-4})
τ	86 400	Length of one day (s)
ξ	0.01	Boundary growth parameter (—)
c_p	1004.67	Specific heat of dry air (J kg^{-1} K^{-1})
c_t	10^{-5}	Surface thermal coefficient (K m^2 J^{-1})
g	9.81	Gravitational constant (m s^{-2})

splitting the daytime into equal time steps (20 for this analysis). The length of the time steps depends on day length and hence latitude and time of year. For reference, the subscript i is used to designate variables calculated at each subdaily time step.

The first assumption made was that the surface latent heat flux is negligible at night and has a daytime profile proportional to the incoming shortwave flux. This allowed us to calculate the latent heat flux at each time step L_i directly from the daily-mean L by assuming it was proportional to the incoming shortwave radiation at each time step,

$$L_i = L\left(\frac{\frac{\mathrm{SW}_{\mathrm{in},i}}{\Delta t}}{\frac{\mathrm{SW}_{\mathrm{in}}}{\tau}}\right), \tag{8}$$

where Δt is time step length, τ is the length of a day (see Table 2 for a complete list of constants), and $\mathrm{SW}_{\mathrm{in},i}$ is the incoming solar radiative flux calculated at each time step. For most situations, this yielded reasonable results (section 3). However, it was incapable of capturing influences that cause the daytime evolution of latent heat flux to deviate from the radiative profile, including phenomena such as midday stomata closure and desert plant transpiration where significant evapotranspiration may occur at night.

To address the influence of G at subdaily time steps, we used the formulation of Friedl (Friedl 2002). In this method the surface heat storage depends on sun angle φ, leaf area index LAI, and full spectrum net radiation $R_{\mathrm{net},i}$,

$$G_i = 0.3R_{\mathrm{net},i}\exp\left[\frac{-0.5\mathrm{LAI}}{\cos(\phi)}\right]\cos(\phi). \tag{9}$$

Although numerous other formulations for G exist (Kustas and Daughtry 1990; Santanello and Friedl 2003; Liebethal and Foken 2007), this method is most appropriate here because of its explicit dependence on leaf area that implies a dependence on land-cover type.

2.2.2. Diurnal variation of longwave and sensible heat fluxes

With subdaily formulations for G, L, $\mathrm{SW}_{\mathrm{in}}$, and $\mathrm{SW}_{\mathrm{out}}$ described above, an expression for $R_{n,i}$ or H_i is needed to close the subdaily surface energy balance,

$$H_i = \mathrm{SW}_{\mathrm{out},i} - \mathrm{SW}_{\mathrm{in},i} - R_{n,i} - L_i - G_i. \tag{10}$$

Using G_i calculated using (9), the diurnal evolution of surface temperature was estimated using a force–restore method proposed by Bhumralkar (Bhumralkar 1975) and Blackadar (Blackadar 1976),

$$\frac{\partial T_{s,i}}{\partial t} = c_t G_i - \frac{2\pi}{\tau}(T_{s,i} - T_m). \tag{11}$$

Although the surface thermal coefficient c_t is generally a complicated function of soil moisture, soil texture, and vegetative properties, for simplicity we assume the coefficient to be constant. Using the surface temperature calculated in (11), the net longwave radiation at each time step can be determined by

$$R_{n,i} = R_{gu,i} - (1 - \epsilon_{bl,i})R_{fd,i} - R_{bd,i}, \tag{12}$$

with

$$R_{gu,i} = \epsilon_s \sigma (273.15 + T_{s,i})^4, \tag{13}$$

where ε_{bl} is the effective column emissivity of the ABL and is a function of pressure and moisture. The term $R_{fd,i}$ is the downwelling longwave radiation from the free atmosphere, and $R_{bd,i}$ is the downwelling longwave radiation emitted from the ABL (Figure 2). The expressions for ε_{bl}, $R_{fd,i}$, $R_{bd,i}$, and the corresponding upwelling ABL component ($R_{bu,i}$) were derived from Brutsaert's (Brutsaert 1975) calculation of effective atmospheric emissivities (refer to Kim and Entekhabi 1998 for their formulations). Calculation of $R_{n,i}$ using Equation (12) allowed closure of the surface energy balance, and the sensible heat flux at each time step H_i could be calculated as the residual of Equation (10).

To reconcile the subdaily values of H_i and G_i needed for ABL calculations with the daily-mean values calculated in the PEGASUS land model, two assumptions were made. First, the nighttime sensible heat flux (generally negative) was such that the daily mean of H_i equals H. The second assumption was that the nighttime heat storage was equal and opposite to the daytime heat storage, such that G_i averaged over a 24-h period was zero. In general the contribution of G to the surface energy balance tends to be small, and under most conditions the assumption that the daily mean of G equals zero is reasonable. However, this assumption limits the utility of this approach in urban and some semiarid landscapes where the imbalance between daytime and nighttime surface energy storage is considerable during parts of the year. Although the focus of this study was daytime evolution of the surface energy balance and boundary layer dynamics, further development of the nighttime formulations may lead to improved model performance in future work.

2.2.3. Boundary layer dynamics

Subdaily ABL height was estimated based on surface forcings of latent heat, sensible heat, and longwave radiate energy [Equations (8), (10), and (13)]. As these forcings evolve throughout the day, the height of the ABL changes. The rate of change of the ABL height z_i under convective conditions was given by Kim and Entekhabi (Kim and Entekhabi 1998) as

$$\frac{dz_i}{dt} = \frac{2\theta G_* e^{-\xi z_i}}{g z_i \delta_\theta} + \frac{0.2 H_v}{\rho c_p \delta_\theta} \quad \text{and} \tag{14}$$

$$G_* = U_*^2 U, \tag{15}$$

where the subscript i has now been dropped for convenience and all terms are assumed to be calculated at each time step. In Equation (14), the first term represents mechanically generated turbulent growth and is a function of θ, z, wind speed U, frictional velocity U_*, the difference in θ between the free atmosphere and ABL δ_θ, and constants g and ξ (Table 2). The second term is ABL growth due to surface virtual heat flux ($H_v \approx H + 0.61 c_p L \rho^{-1}$), weighted by air density ρ, δ_θ, and the constant c_p. When stable conditions existed, z_i was given by Zilitinkevich and Baklanov (Zilitinkevich and Baklanov 2002) as

$$z_i = \frac{0.4 U_*}{f}\left[1 + \frac{0.4^2 U_*(1 + 0.25 L_m N/U_*)}{0.75^2 f L_m}\right], \tag{16}$$

where f is the Coriolis parameter, L_m is the Monin–Obukhov length, and N is the Brunt–Väisälä frequency.

As z_i increases, relatively dry and warm air entrained from the free atmosphere resulted in sensible (H_{top}) and latent (L_{top}) heat fluxes at the top of the ABL (Figure 2). The transition between the ABL and free atmosphere was assumed to have discrete jumps in Q and θ (designated δ_θ and δ_Q), representing the commonly occurring inversion at the top of the mixed layer. In the free atmosphere, we assumed constant gradients and for Q (γ_Q) and θ (γ_θ), which were calculated assuming a standard atmosphere as given by Brutsaert (Brutsaert 1975). Additionally, δ_θ and δ_Q evolved as air from the free atmosphere became entrained into the ABL and surface fluxes altered the state of the ABL. The expressions for δ_θ, δ_Q, H_{top}, and L_{top} are (Margulis and Entekhabi 2001)

$$\frac{d\delta_\theta}{dt} = \gamma_\theta \frac{dz_i}{dt} - \frac{d\theta}{dt}, \tag{17}$$

$$\frac{d\delta_Q}{dt} = \gamma_Q \frac{dz_i}{dt} - \frac{dQ}{dt}, \tag{18}$$

$$H_{\text{top}} = \rho c_p \delta_\theta \frac{dz_i}{dt}, \quad \text{and} \tag{19}$$

$$L_{\text{top}} = \rho \delta_Q \frac{dz_i}{dt}. \tag{20}$$

Finally, with expressions for mixed layer forcings at the top and bottom of the ABL in place and neglecting advected energy and moisture, we calculated the rate of change of θ and Q by considering the following boundary layer budget equations:

$$\frac{d\theta}{dt} = \frac{1}{\rho c_p z_i}\left[(R_{fd} + R_{gu})\epsilon_{bl} - R_{bu} - R_{bd} + H + H_{\text{top}}\right] \quad \text{and} \tag{21}$$

$$\frac{dQ}{dt} = \frac{1}{\rho z_i}(L + L_{\text{top}}), \tag{22}$$

where R_{xx} represents the various radiative fluxes shown in Figure 2.

2.2.4. Boundary layer initial conditions

A primary goal of this study was to test how land cover influenced the daytime surface energy balance and ABL evolution. To accommodate this goal, we initialized the ABL and surface energy model at sunup of each day. We began by assuming the surface temperature to be at a climatological daily minimum provided by CRU 30-yr data,

$$T_{s,\text{init}} = T_m - \frac{\text{dtr}_m}{2}, \tag{23}$$

where dtr_m is the CRU 30-yr monthly-mean diurnal temperature range. We then assumed the initial ABL potential temperature to be initially stable relative to the surface temperature,

$$\theta_{\text{init}} = T_m - \frac{\text{dtr}_m}{1.6 \times 2}. \tag{24}$$

The initial ABL specific humidity was designated to be at the dewpoint, and at the top of the ABL we initialized δ_θ and δ_Q as

$$\delta_\theta = \frac{\text{dtr}_m}{3}, \quad \delta_Q = 500\gamma_Q. \tag{25}$$

We refer to the combined vegetation–surface–atmospheric boundary layer model as PEGASUS boundary layer (PegBL).

3. Model evaluation across biomes

Bulk ABL models have been developed for a variety of applications for several decades (Tennekes 1973). However, these models have generally been implemented at point locations (Troen and Mahrt 1986; Kim and Entekhabi 1998; Gash and Nobre 1997) or as components of climate models' dynamical cores (Randall and Branson 1998). In these applications, large-scale forcing and initial conditions could be precisely specified or modeled. Bulk ABL models are not typically generalized for application over large regions and across climate zones. Here, we evaluated the ability of PegBL to model the soil–vegetation–boundary layer system without inputs from climate models or direct observations by comparing modeled surface fluxes and ABL variables to observations taken at several

Table 3. Summary of observational sites used for verification.

Field campaign/site	Location	Date(s)	Key relevant observations
ABRACOS/RBLE/ LBA field campaign	Amazon rain forest site	1990–94, 1999	Radiosondes, tethersondes, surface flux measurements, surface radiation
BOREAS field campaign	Saskatchewan and Manitoba boreal forest sites	1993, 1994, 1996	Radiosondes, RASS boundary layer measurements, surface radiation, eddy-correlation surface flux measurements, intermittent aircraft measurements
FIFE field campaign	Kansas prairie grassland site	1987–89	Radiosondes, surface radiation, surface flux measurements, aircraft measurements
HAPEX field campaign	West African Sahel site	1991–93	Radiosondes, eddy-correlation surface flux measurements, intermittent aircraft observations
WLEF tall tower observations	Northern Wisconsin mixed forest	Flux observations are ongoing, and boundary layer observations are for March–November 1999	National Center for Atmospheric Research (NCAR) Integrated Sounding System, sonic anemometers and infrared spectroscopic measurements (Li-COR Biosciences, Inc. LI-6262) of water vapor and CO_2 to derive surface fluxes.

field campaign and flux tower sites across the globe and across a wide variety of environmental conditions.

Field campaigns routinely have dissimilar observational equipment and goals, which makes direct comparison among the sites and to model data difficult. Additionally, each site has its own idiosyncrasies that must be accounted for. Finally, field experiments are generally conducted over relatively short periods during which weather conditions may not resemble climatology. For this study, we selected five field sites that represented a range of biomes, have detailed flux surface data, and reported direct observations of some of the ABL state variables (z_i, θ, and Q). The site descriptions are summarized in Table 3. We present the results of these comparisons in sections 3.1–3.5 and discuss the implications in section 3.6.

3.1. PegBL–BOREAS comparison

The Boreal Ecosystem–Atmosphere Study (BOREAS) experiment represented a concentrated effort to improve understanding of the boreal forest biome and its exchanges of energy, water, and carbon with the atmosphere (Sellers et al. 1997). This experiment ran from 1993 to 1997 and included intensive field campaigns (IFCs) in 1994 and 1996. The boreal biome was particularly interesting for our purposes not only because it occupies a relatively large proportion of Earth's surface but also because it has been identified by multiple studies as a region where land-use change can have large impacts on local climate (Bonan et al. 1992; Betts 2000; Snyder et al. 2004; Davin and de Noblet-Ducoudré 2010).

The BOREAS project was constrained to two 50 km × 50 km regions called the northern and southern study areas. These regions were located near Thompson,

Manitoba, and Prince Albert, Saskatchewan, respectively. They were chosen for their proximity to the north and south ecotones of boreal forest biome (Sellers et al. 1997). In general, these regions were characterized by aspen, jack pine, and black spruce tree cover interspersed with wetlands. Here, we focused on data from an Old Jack Pine site located within the southern study area (~53.8°N, 105.27°W). This site was somewhat unique in the BOREAS experiment because of the existence of relatively continuous long-term z_i observations via a radio acoustic sounding system (RASS), which was deployed from 21 May through 20 September 1994 in conjunction with flux tower measurements that provided surface flux observations (Wilczak 1999). Combined, these observations provided us with a long continuous dataset that was suitable for model evaluation.

We compared PegBL's June–September z_i and surface fluxes to BOREAS observations in Figures 3a–d. Although PegBL overestimated the latent and radiative surface fluxes in June and July, it did capture the seasonal reduction in surface fluxes as fall began. The surface sensible heat flux, which strongly influenced the daily ABL evolution, was more accurately modeled relative to its magnitude. As shown in Table 4, the mean absolute error (MAE) for H ranged from 44 W m^{-2} in June to 35 W m^{-2} in September, well within observed daily variations that had monthly standard deviations ranging from 113 W m^{-2} in June to 71 W m^{-2} in September. One limitation of our simple sensible heat flux formulation was that it caused the early morning flux to increase too quickly in PegBL compared to observations. This was reflected in the modeled z_i (Figure 3d), where the boundary layer rises earlier than found in the RASS observations. However, the late day and maximum z_i were within observed day-to-day variability throughout the observation period. Thus, in spite of the fact that PegBL was driven by climatological data and neglected advected heat and moisture, we found the model adequately reproduced the evolution and magnitude of daytime surface fluxes and z_i for this BOREAS location throughout the boreal summer.

As part of the BOREAS experiment, radiosondes were launched throughout the southern study area for 32 days from May to September 1994. Barr and Betts (Barr and Betts 1997) made a composite of these soundings to estimate mean daytime ABL profiles. PegBL was able to simulate the magnitude and evolution of z_i (Figure 4). Also, the daily variation and magnitude of specific humidity was accurate to 0.001 kg kg^{-1}, with entrainment of dry air from the free atmosphere causing a decrease in Q throughout the day. The 6–7-K daily variation of θ was captured, and the magnitude reproduced within 3 K. This gave us confidence that PegBL was reproducing the key features of the boreal forest's surface flux and ABL response, despite the simplicity of our approach. Finally, Figure 4 illustrates that, even with high intramonthly variability in the ABL, PegBL closely approximates the field observations of turbulent heat fluxes.

3.2. PegBL–WLEF tower comparison

The second site selected for comparison was the WLEF flux tower in the Chequamegon Forest in northern Wisconsin (45.95°N, 90.27°W) (Bakwin et al. 1998; Davis et al. 2003; Yi et al. 2004; Desai et al. 2010). The flux tower was located in a grass clearing surrounded by mixed forest. Sonic anemometers were

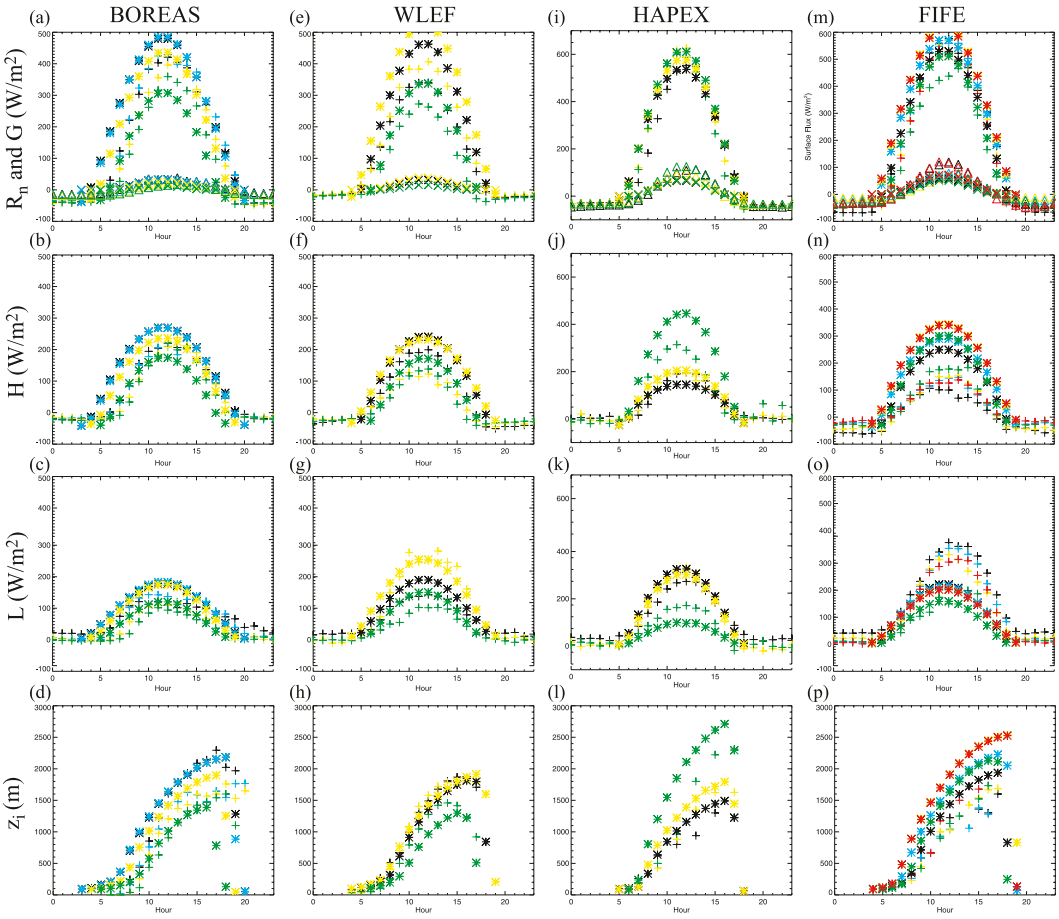

Figure 3. Observed (crosses) and modeled (asterisks) surface fluxes and z_i for (a)–(d) the BOREAS old jack pine site, (e)–(h) the WLEF tall tower site, (i)–(l) the HAPEX-Sahel fallow savanna site, and (m)–(p) the FIFE site. (a),(e),(i),(m) Modeled surface energy storage is denoted with Xs and observed with triangles. There were no surface energy storage observations available for the WLEF site. For the BOREAS site, the data shown are monthly means from June (black), July (blue), August (yellow), and September (green). At WLEF, the data shown represent seasonal means for April–May (black), June–August (yellow), and September–October (green). For the HAPEX site, the data represent monthly means from August (black), September (yellow), and October (green). Finally, for FIFE, each color represents an IFC such that IFC-1 is black, IFC-2 is blue, IFC-3 is yellow, IFC-4 is green, and IFC-5 is red.

located on the tower at 30, 122, and 396 m. The anemometers measured turbulent winds and virtual potential temperature. Using these measurements and IR gas analyzer observations of H_2O, the surface fluxes were estimated using eddy-correlation techniques (Baldocchi et al. 1997). Bakwin et al. (Bakwin et al. 1998) and Berger et al. (Berger et al. 2001) provide detailed descriptions of the instrumentation and flux calculations at the site. From April to October 1999, Yi et al. (Yi et al. 2004)

Table 4. The MAE for PegBL modeled surface fluxes and boundary layer variables vs values observed at the sites described in section 3. The values in parentheses represent the MAE for PegBL when forced by CRU data from the actual year that observations for a site were taken as opposed to climatology.

	BOREAS MAE			
	Jun	Jul	Aug	Sep
H (W m^{-2})	44.38 (25.59)	48.01 (23.01)	39.12 (36.47)	35.49 (36.24)
L	42.28 (42.16)	29.22 (30.90)	41.31 (35.32)	22.3 (21.25)
R_n	56.32 (36.43)	57.44 (42.94)	54.43 (50.14)	43.43 (44.56)
G	7.27 (8.76)	7.63 (8.44)	7.81 (7.55)	7.51 (7.54)
z_i (m)	201 (358)	452 (219)	347 (243)	257 (261)

	WLEF MAE						
	Apr	May	Jun	Jul	Aug	Sep	Oct
H (W m^{-2})	34.3 (16.3)	40.2 (18.5)	71.4 (30.6)	73.7 (28.9)	59.1 (31.9)	43.2 (20.1)	17.8 (15.9)
L	42.8 (33.2)	39.8 (21.9)	34.7 (21.9)	59.0 (62.6)	20.7 (21.4)	20.3 (12.3)	31.6 (20.7)
R_n	61.9 (14.4)	94.7 (35.0)	93.9 (27.0)	80.4 (35.1)	103.0 (54)	45.6 (18.4)	55.8 (24.7)
z_i (m)	72 (326)	150 (411)	118 (400)	114 (290)	109 (280)	179 (346)	229 (386)

	HAPEX MAE		
	Aug	Sep	Oct
H (W m^{-2})	25.16 (23.34)	22.3 (39.31)	113.57 (139.89)
L	54.87 (46.38)	17.4 (25.41)	42.72 (53.88)
R_n	45.44 (44.06)	37.68 (37.24)	53.24 (69.80)
G	31.63 (32.19)	18.12 (18.17)	29.95 (28.55)
z_i (m)	142.54 (146.65)	193.4 (241.24)	503.42 (596.73)
θ (K)	3.33 (2.09)	2.28 (2.00)	3.59 (3.68)
Q (kg kg^{-1})	0.0149 (0.0149)	0.0136 (0.0136)	0.0122 (0.0122)

	FIFE MAE				
	IFC-1	IFC-2	IFC-3	IFC-4	IFC-5
H (W m^{-2})	116.1 (55.7)	112.0 (21.5)	154.2 (94.2)	89.9 (15.9)	164.541 (65.1)
L	80.9 (90.5)	78.3 (61.9)	71.6 (78.3)	32.9 (50.6)	69.2 (49.2)
R_n	30.7 (95.7)	38.0 (58.4)	75.3 (44.5)	53.6 (29.4)	91.5 (46.3)
G	31.7 (38.6)	7.3 (12.0)	10.2 (5.8)	15.8 (18.7)	24.3 (31.0)
z_i (m)	121.8 (150.4)	670.1 (295.3)	1018.2 (483.0)	167.4 (123.2)	902.3 (261.4)
θ (K)	4.0 (4.1)	6.4 (6.2)	2.2 (2.2)	4.6 (3.7)	2.1 (1.6)
Q (kg kg^{-1})	0.005 (0.005)	0.022 (0.022)	0.024 (0.023)	0.002 (0.001)	0.029 (0.028)

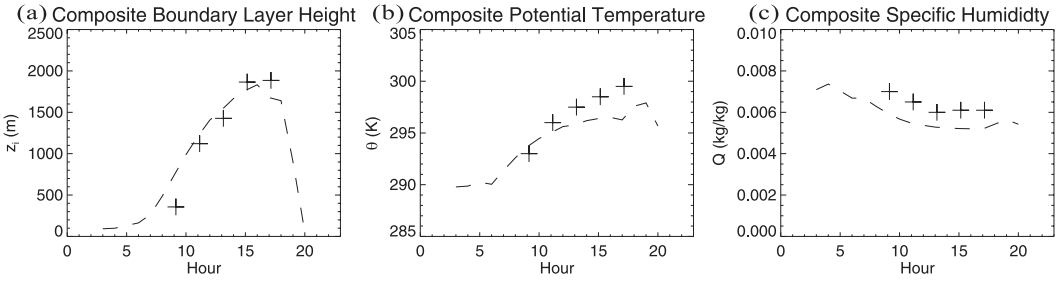

Figure 4. Observed (crosses) and modeled (dashed line) (a) boundary layer height, (b) potential temperature, and (c) specific humidity for the BOREAS southern study area. Observed values are estimated from Barr and Betts's southern study area composite boundary layer profiles for the entire BOREAS study period (1997). These graphs represent the June–September mean z_i, θ, and Q for the entire southern study area. The modeled results mirror observed values within what would be expected from interannual variability.

measured z_i near the site using tower CO_2 concentration measurements and an integrated sounding system, which included a RASS unit.

Figures 3e–h compare surface fluxes and z_i observed at the WLEF tower with PegBL results and MAE for the site is given in Table 4. Although the diurnal variation of z_i was accurately modeled throughout the experiment with the MAE ranging from 72 to 150 m, the net radiation was excessive in May through August (MAE ranging from 46 to 103 W m^{-2}). There are several possible sources for the discrepancy in net radiation. First, the albedo of mixed forests can vary widely across space, which could strongly impact the net radiation. Additionally, this flux tower was centered within a clearing, which one would expect to increase albedo and decrease the net radiation. Interannual variability also appears to play a role, with the cloud cover in 1999 being more extensive than the climatological mean for the WLEF tower location. When we used the 1999 CRU reanalysis of Mitchell and Jones (Mitchell and Jones 2005) to force PegBL, as opposed to the 30-yr mean climatological datasets described above, the discrepancy in net radiation disappeared and other surface fluxes more closely resembled the observations (MAE ranged from 14 to 54 W m^{-2}). This could largely be attributed to increased cloud cover of 14%–22% over the analysis period in the 1999 dataset relative to the 30-yr mean dataset. This finding suggests that care must be taken when interpreting comparisons of the climatologically driven PegBL with observations from point locations for a limited time period and that interannual variability of highly variable quantities such as midlatitude cloud cover and rainfall can significantly influence results.

3.3. PegBL–HAPEX-Sahel comparison

From mid-1990 to late 1992, the Hydrological and Atmospheric Pilot Experiment in the Sahel (HAPEX-Sahel) was conducted in western Niger (~13°N, 2°E), with an 8-week intensive study period occurring from the mid to late growing

season (August–October) in 1992 (Goutorbe et al. 1994). The general goal of this experiment was to understand the impact of land surface variations in the Sahel on the general circulation of the atmosphere and how this influences droughts in the region.

Similar to the BOREAS experiment, HAPEX-Sahel observations were designed to capture land–atmosphere phenomena occurring on scales ranging from the microscale to mesoscale. Intensive study period observations included surface flux measurements and atmospheric radio soundings at three supersites representative of the region (Dolman et al. 1997). The existence of these observations, the uniquely strong influence of land cover on the region, and the strong seasonal shift in rainfall and temperature associated with movement of the intertropical convergence zone (ITCZ) during the Sahel's growing season made this an important comparison point for PegBL.

The region covered by the HAPEX-Sahel experiment was characterized as a savanna. It also had areas that were significantly cultivated. During the intensive study period of 1992 the precipitation and vegetative state of the region was near the climatological mean (Goutorbe et al. 1994).

For the HAPEX-Sahel experiment, we focused on radiosonde, radiative, and surface flux observations from the southern supersite that was characterized as a fallow savanna and was designed to measure late growing season (August–October) surface energy balance fluctuations. For August in this region of the Sahel, the wet season is nearing its end and the latent heat flux is very large. By September, the ITCZ has moved to the south of this region and rainfall drops precipitously. This was reflected in surface fluxes as the Bowen ratio became greater than one in October as the sensible heat flux dominated the surface balance. PegBL reproduced the late growing season evolution of surface fluxes, although the magnitude of the shift in Bowen ratio was larger than observed with the dominating latent heat flux being too large in August and sensible heat flux being too large in October (Figures 3j,k). The rise of the sensible heat flux directly impacted the observed and modeled potential temperature, specific humidity, and z_i (Figures 5a,b) with the mean potential temperature increasing by ~3 K, the mean specific humidity decreasing by ~4 kg kg^{-1}, and the maximum z_i rising by ~1000 m. Unlike the WLEF site, forcing PegBL with the 1992 CRU data of Mitchell and Jones (Mitchell and Jones 2005) did not appreciably change the results or the MAE (Table 4). This was due to the 1992 data closely resembling the climatological reanalysis for this location during the analysis time period. Thus, the discrepancies in the surface heat flux and ABL properties were likely due to a combination of limitations in PegBL's soil physics and precipitation in the region generally falling in localized convective storms that the monthly-mean datasets used in PegBL smooth out.

3.4. PegBL–FIFE comparison

The First International Satellite Land Surface Climatology Project (ISLSCP) Field Experiment (FIFE) was conducted from 1987 to 1989 near the Konza Prairie Long Term Ecological Research site. FIFE was intended as an experiment to understand the role biology has in influencing land–atmosphere interactions and determining the usefulness of satellites for climatological land surface studies

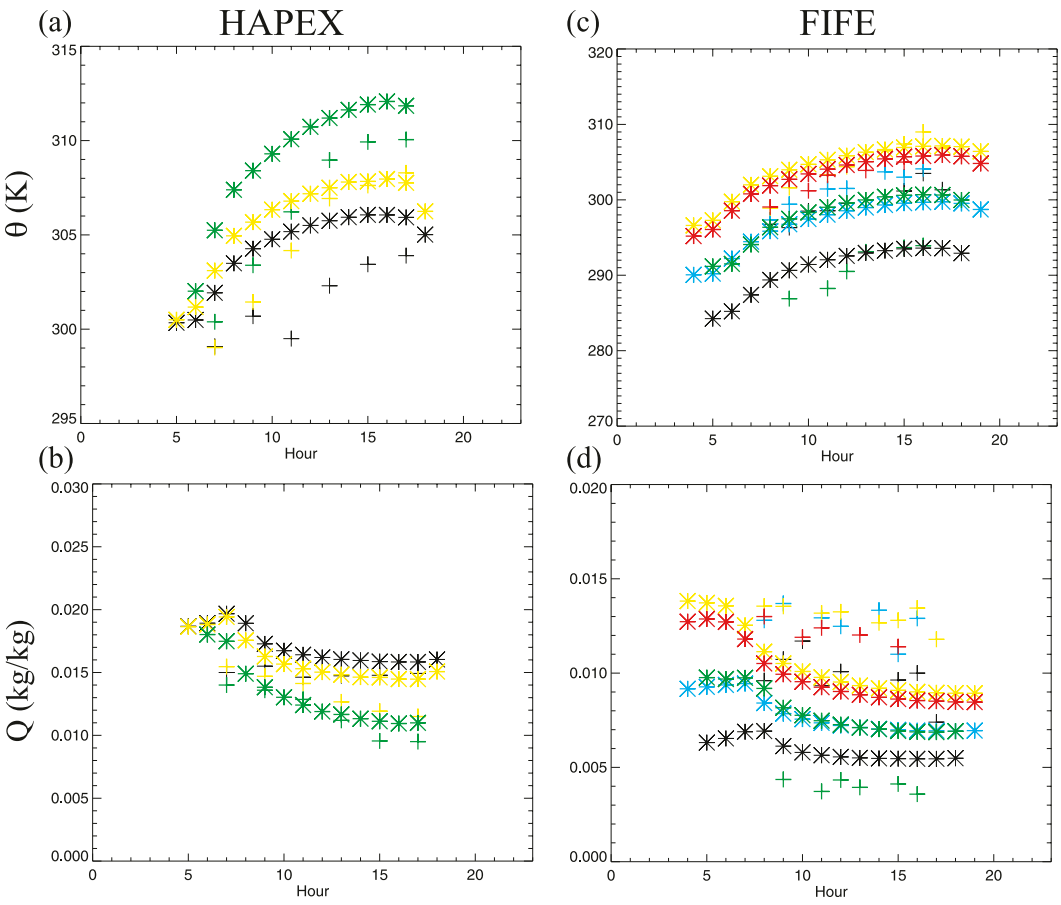

Figure 5. Observed (crosses) and modeled (asterisks) θ and Q at (a),(b) the HAPEX-Sahel fallow savanna site and (c),(d) the FIFE site. For the HAPEX site, the data shown are monthly means from August (black), September (yellow), and October (green). For FIFE, each color represents IFC such that IFC-1 is black, IFC-2 is blue, IFC-3 is yellow, IFC-4 is green, and IFC-5 is red.

(Sellers et al. 1988). As a result of these experimental objectives, surface flux and ABL observations were taken.

The observational site was a 15 km × 15 km region centered on 39.05°N, 96.53°W near Manhattan, Kansas. The land cover in the region was primary characterized as grassland. Although surface flux measurements were taken throughout the growing season months of 1987 and 1988, intensive radiosonde atmospheric observations taken near the northern border of the study region were constrained to a series of four IFCs in 1987 and one in 1989. The first IFC in 1987 (IFC-1) ran from 26 May to 6 June, the second (IFC-2) ran from 26 June to 11 July, the third (IFC-3) ran from 6 to 21 August, and the final 1987 IFC (IFC-4) ran from 5 to 16 October. The fifth IFC (IFC-5) ran in 1989 from 25 July to 12 August (Betts and Ball 1998). These IFCs were designed to capture the major phases of vegetation in the region: 1) the greening of the vegetation, 2) the peak greenness, 3) a dry down period, and 4)

senescence. However, unusual weather conditions in 1987 for the region resulted in very similar conditions for the first three IFCs (missing the dry down) and unusually dry soil and senescence for the fourth IFC (Betts and Ball 1998). The fifth IFC in 1989 was created to try to capture the dry down period missed in 1987.

PegBL simulations of surface fluxes and ABL variables revealed immediate discrepancies (Figures 3m–p, 5c,d). PegBL's net radiation tended to be too high and its surface heat storage tended to be too low. More egregiously, the Bowen ratio was greater than one for every IFC, with the sensible heat flux being consistently overestimated. This was reflected in modeled z_i that were too high with an MAE range from 122 to 1018 m (Table 4). Figures 3m–p and 5c,d also appear to illustrate the difficulty of comparing observations from the relatively short IFCs with model output designed to simulate climatological mean values, as the ABL potential temperature and specific humidity alternated between values that were too high and too low relative to observations.

When we compared the 30-yr mean CRU reanalysis of New et al. (New et al. 2002) with the 1987 and 1989 CRU data of Mitchell and Jones (Mitchell and Jones 2005) and the FIFE precipitation estimates from Betts and Ball (Betts and Ball 1998), we found that the year-specific data had significantly increased cloud fraction and precipitation. When these datasets were used as inputs to PegBL, the modeled surface fluxes and ABL improved significantly (MAE from 123 to 483 m) (Table 4, S1). Although the modeled net radiation became slightly underestimated for IFC-1 and IFC-2, the latent heat flux increased throughout the observational period causing the Bowen ratio to shift toward the observed values for all IFCs. In the ABL, the issue of the mixed layer height being overestimated relative to FIFE observations was ameliorated, and specific humidity estimates were improved. These results highlight the role interannual variability can play. At the FIFE site, a combination of relatively short observational times and nonclimatological conditions over the study periods caused our model to deviate from observations.

3.5. PegBL–LBA comparison

The final site selected for model comparison was located in the tropical rain forest of the Ji-Parana region of Brazilian Amazonia. In the early 1990s, the Anglo-Brazilian Amazonian Climate Observation Study (ABRACOS) and Rondonia Boundary Layer Experiment (RBLE) field campaigns were launched as precursors to the Large-Scale Biosphere–Atmosphere Experiment in the Amazon (LBA) (Gash and Nobre 1997; Culf et al. 1996). These field campaigns were somewhat unique in that a primary component of them was to detect differences in surface and ABL variables between forested land and land converted to pasture. To do this, observations were concurrently taken in close proximity ($\sim<$100 km) at paired forested and pasture sites. This emphasis on land-use change made these observations ideal for our purposes.

In this region of the Amazon, the temperature is fairly constant throughout the year, but there are distinct wet and dry seasons. Generally, the dry season lasts from July to September and the wet season lasts from January to March. During the wet season, the climatological precipitation rate is nearly 300 mm month^{-1} (Fisch et al. 2004). As the dry season arrives with the ITCZ moving out of the region, this

rate drops to less than 50 mm month^{-1} with most of that precipitation coming from very intermittent cold air weather systems known as friagems. On the whole, the atmospheric forcing on this region during the dry season is small, allowing land-cover change to have a relatively unperturbed influence on the boundary layer circulation and making this a particularly good test case for our model. This region also has minimal influences from oceans and topography.

The first site was located at 10°5′S, 61°55′W in an undisturbed tropical forest, with the surrounding area being 95% undisturbed forest. This site was initially developed in 1991 as part of the ABRACOS experiment and measured surface meteorological and turbulent fluxes on a 47-m tower (Fisch et al. 2004). Additionally, during the RBLE in August 1993, dry season daytime ABL measurements were taken at 0800, 1100, 1400, and 1700 local time via rawinsondes near the tower. In January–February 1999, daytime balloon launches were again taken as part of LBA in order to investigate wet season impacts.

According to von Randow et al. (von Randow et al. 2004), the pasture site was located on a cattle ranch at 10°45′S, 62°21′W. The area was initially burned in 1977, was 4 km wide and tens of kilometers long, and was situated within a cleared 50-km area that was largely (90%) deforested. Measurements taken at this site mirror the forested site closely. More information on the equipment used for surface flux and ABL measurements can be found in von Randow et al. (von Randow et al. 2004) and Fisch et al. (Fisch et al. 2004).

For the wet (January–March) season, we found relatively small differences between forest and pasture sites for both observed and modeled surface fluxes (Figure 6). The net radiation at the forested location was slightly larger than the pasture site because of its lower albedo. Most of the increase in incoming energy was balanced by a corresponding increase in latent heat flux, with the sensible heat flux changing only slightly. During the dry season (July–September), we found more obvious changes in the surface energy balance (Figures 6a–c,h–j). At the forest site, there was a strong modeled and observed increase in latent heat flux relative to the pasture site because of the tropical rain forest's ability to access moisture far below the surface during the dry season (von Randow et al. 2004). Accompanying the increase in latent heat flux at the forested site was a corresponding decrease in sensible heat flux as required by the surface energy budget (assuming small changes in net radiation).

The changes in surface fluxes have direct consequences on ABL state variables in the Ji-Parana region (Figures 6d–f,k–m). During the wet season only small differences existed between the pasture and forested sites in PegBL's modeled ABL and observations. However, the dry season brought lower potential temperature, higher specific humidity, and a lower z_i at the forested site because of the increased latent heat flux and lowered sensible heat flux in both the model and observations. This gives us confidence that PegBL was accurately representing the impact of land-use change in the tropical rain forest.

3.6. Implications of site comparisons and model uncertainty

Inasmuch as the comparisons of the preceding sections were indicative of overall model performance, several inferences can be drawn. First, interannual variability cannot be ignored when comparing PegBL to observations. In both the FIFE and

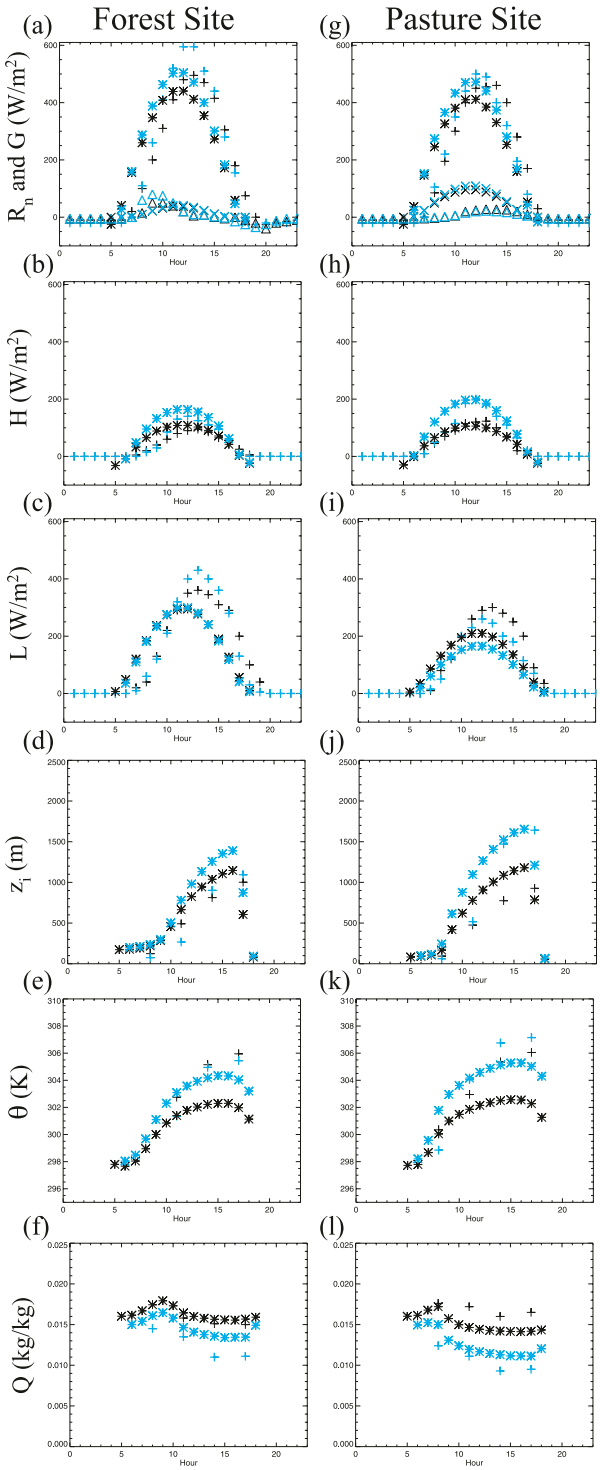

Figure 6. Observed (crosses) and modeled (asterisks) (a)–(c),(g)–(i) surface fluxes; (d),(j) z_i; (e),(k) θ; and (f),(l) Q for the dry (blue) and wet (black) seasons for the (a)–(f) forest and (g)–(l) pasture LBA sites. (a),(g) PegBL-modeled G is denoted with Xs and observed G is denoted with triangles. (c),(i) PegBL reproduced the large changes in L associated with forest conversion in the dry season and relatively small changes in the wet season.

WLEF comparisons, cloud cover and precipitation differed significantly from climatological values. This had direct consequences on PegBL's surface energy balance and hence its ABL state variables. However, sites such as BOREAS that had longer, more continuous records of the ABL tended to better match modeled results, as did the LBA and HAPEX sites where observed conditions closely resembled climatology. These results indicate that mean climatology works as a base state for modeling the soil–vegetation–boundary layer system of regions over sufficiently long periods. Additionally, as the LBA comparison demonstrated, when perturbations to the overall climate due to land-use change are small, mean climatology is a valid base state for modeling the impact of land use on the surface energy balance and ABL. However, the use of climatology as a base state may limit PegBL's applicability in places influenced by large long-term variability, such as regions strongly impacted by El Niño.

These comparisons also indicate that PegBL may capture the dynamics of some biomes and variables more realistically than others. In general, the observed daily evolution and magnitude of the ABL state variables z_i, θ, and Q were well reproduced when surface fluxes were accurately modeled. However, the accuracy of the surface fluxes differed across biomes and were influenced by interannual variability. Drawing from the results of BOREAS and LBA, PegBL did well modeling the surface energy balance and ABL dynamics of tropical and boreal forest biomes. In the grassland (FIFE) and savanna (HAPEX-Sahel), the features of gross seasonal changes in surface energy balance and ABL variables were captured. However, within these seasonal changes, discrepancies between the modeled and observed variables were clear, calling into question the model's representation of the surface energy balance in these regions.

Along with interannual variability, the discrepancies between modeled and observed variables may be partly attributed to uncertainties in the model. There were several uncertainties in our approach that could contribute to systematic differences in observational comparisons. The horizontal advection of moisture, energy, and z_i were neglected within the ABL. The comparisons of the previous sections were primarily carried out in spatially homogenous regions, which should reduce the impact of advection. However, in regions such as coastlines where consistent temperature and moisture gradients exist, errors are likely to arise. WE10 noted several regions where the regional transport of heat and moisture was stronger than local forcing from the land surface. Also, in the ABL, the initialization of the jumps in θ and Q between the ABL and free atmosphere gradient were designed to provide reasonable results across a variety of conditions but may not be appropriate for some locations, particularly regions of large-scale subsidence. Finally, there are no mechanisms for lateral groundwater transport in PegBL, which could result in changes in the availability of water for evapotranspiration and hence the surface energy balance. These could be incorporated but at the expense of our simplified experimental design.

4. Potential biogeophysical impact of land-cover change on surface fluxes and the boundary layer

The results of the previous section indicate that PegBL can reproduce key features of observed surface fluxes and the state of the ABL for a range of

Table 5. The impact of vegetation removal on sensible heat flux *H*, latent heat flux *L*, net radiation R_n, near-surface air temperature *T*, specific humidity *Q*, and boundary layer height z_i for PEGASUS and previous GCM studies for the Amazon and North American boreal forest regions.

Study	H (W m^{-2})	L (W m^{-2})	R_n (W m^{-2})	T (K)	Q (g kg^{-1})	z_i (m)
			Amazon rainforest			
PEGASUS	+26	−35	−10	+0.89	−1.79	+197
Snyder et al. 2004	+14.7	−33	−18	+1.5	−1.7	+94.9
Shukla et al. 1990	+12	−38	−26	+2.5	—	—
Zhang et al. 1996	+1.6	−17.8	−16.3	+0.3	—	—
			North American boreal forest			
PEGASUS	−12	−12	−22	−2.5	−0.29	−170
Snyder et al. 2004	−6.8	−7.8	−13.3	−2.2	−0.3	−200

environmental conditions, as well as estimate the impact of land-cover change. Here, we investigate global patterns of the local potential impact of vegetation on surface fluxes and the ABL.

Changing the land cover in the model creates several uncertainties in addition to those described in previous sections. One major uncertainty that is not accounted for in PegBL is how land-cover change may influence the stability of the lower atmosphere. Changes in the stability could alter cloudiness and precipitation over a region, which were not addressed in the model. Regional circulation patterns could also shift as local stability changes. If changes in circulation patterns are extensive and persist over long periods, they could violate our assumption that land-cover change is a small perturbation on the global climate.

With the above caveats in mind, we estimated a maximal potential impact of vegetation by running two global land-cover scenarios with PegBL. In the first scenario, we assumed the land cover is described by the potential vegetation dataset discussed in Ramankutty and Foley (Ramankutty and Foley 1999). In the second scenario, all vegetation was converted to bare soil. Although this is an extreme scenario that violated our assumption of land-cover change being a small perturbation on the global climate, the use of climatological reanalysis precipitation and temperature as model input caused changes in circulation to be ignored. Coupled with the model's neglect of advection, we were left with global maps of the local ABL response to land-cover change. Therefore, although neither of these scenarios is realistic, they do provide us with bounds on the potential local influence of natural vegetation.

When potential vegetation was replaced by bare soil, the surface albedo generally increased while transpiration and surface roughness were reduced. This had a direct impact on net radiation, latent heat flux, sensible heat flux, and the surface energy storage (Table 5, S2). Unsurprisingly, the regions where surface fluxes were most affected by the conversion to bare soil were those with the most robust vegetation: the boreal forest and tropical rain forest.

In the tropics, the decrease in net radiation was offset by the decrease in latent heat flux due to transpiration. The result was a slight increase in surface heat storage and a strong increase in sensible heat flux [Equation (2)]. Conversely, in the boreal forest effects due to increased albedo were dominant, because highly reflective snow was uncovered by the removal of radiatively dark trees during winter months. Here, the decrease in latent heat flux was not substantial enough to offset

the change in net radiation, causing a sharp decrease in sensible heat flux. These results from the computationally inexpensive PegBL are comparable and remarkably consistent with previous GCM studies for the tropics (Shukla et al. 1990; Zhang et al. 1996; Snyder et al. 2004) and boreal regions (Table 5) (Snyder et al. 2004). As shown in Table 5, we found that for all boundary layer variables PegBL reproduced not only the correct sign of change for devegetation scenarios but also the mean value of GCM simulations in the tropical rain forest within 16.6 W m^{-2} for surface fluxes, 0.54 K for boundary layer temperature, 0.09 g kg^{-1} for specific humidity, and 102.1 m for boundary layer height. In the boreal forest, magnitudes were reproduced within 8.7 W m^{-2} for surface fluxes, 0.3 K for boundary layer temperature, 0.01 g kg^{-1} for specific humidity, and 30 m for boundary layer height. Combined, these results give confidence that in spite of our simplified physics and dynamics our model has captured the key processes of land-cover change that impact surface fluxes and the ABL.

Modifications to the ABL are associated with the potential impact of vegetation on surface fluxes (Table 5, S3). These modifications arise both from changing surface fluxes and the reduction of surface roughness associated with vegetation. In general, during daytime convective conditions, the changes in ABL growth and temperature associated with land-cover change were most strongly influenced by the changes in sensible heat flux. Thus, in the boreal forest there was a strong reduction in z_i and θ. In the tropics, a moderate increase in θ and z_i occurred, mirroring the sensible heat flux sign. Globally, the specific humidity decreased in the boundary layer as the transpiration source was removed when vegetation is replaced by bare soil.

As discussed in WE10, one constraint of this methodology was that the influence of advection on the ABL was ignored. In some cases, changes in the biogeophysical forcing of vegetation on ABL climate may be insignificant when compared to advective forcings. To estimate the relative influence of biogeophysical regulation of the ABL, WE10 developed simple indices for estimating the biogeophysical regulation of air temperature (θ_{index}) and moisture (q_{index}),

$$\theta_{\text{index}} = \Delta\theta \frac{|\Delta\theta|}{|\Delta\theta| + |\Delta\theta_{\text{adv}}|} \quad \text{and} \tag{26}$$

$$q_{\text{index}} = \Delta q \frac{|\Delta q|}{|\Delta q| + |\Delta q_{\text{adv}}|}, \tag{27}$$

where $\Delta\theta$ and Δq are the changes in ABL potential temperature and moisture due to removal of vegetation and $\Delta\theta_{\text{adv}}$ and Δq_{adv} represent advective forcings. These forcings were estimated using the climatological National Centers for Environmental Prediction (NCEP) reanalysis (Kalnay et al. 1996) and followed the procedure laid out in WE10. In WE10's analysis of biogeophysical regulation, they assumed an extremely simplified box model of the ABL wherein z_i was constant in time and depended only on latitude. Using PegBL with the dynamic boundary layer described above, we refined their estimate.

Comparing our estimates of biogeophysical regulation with estimates following the procedure of WE10, similar patterns arose, with the tropical rain

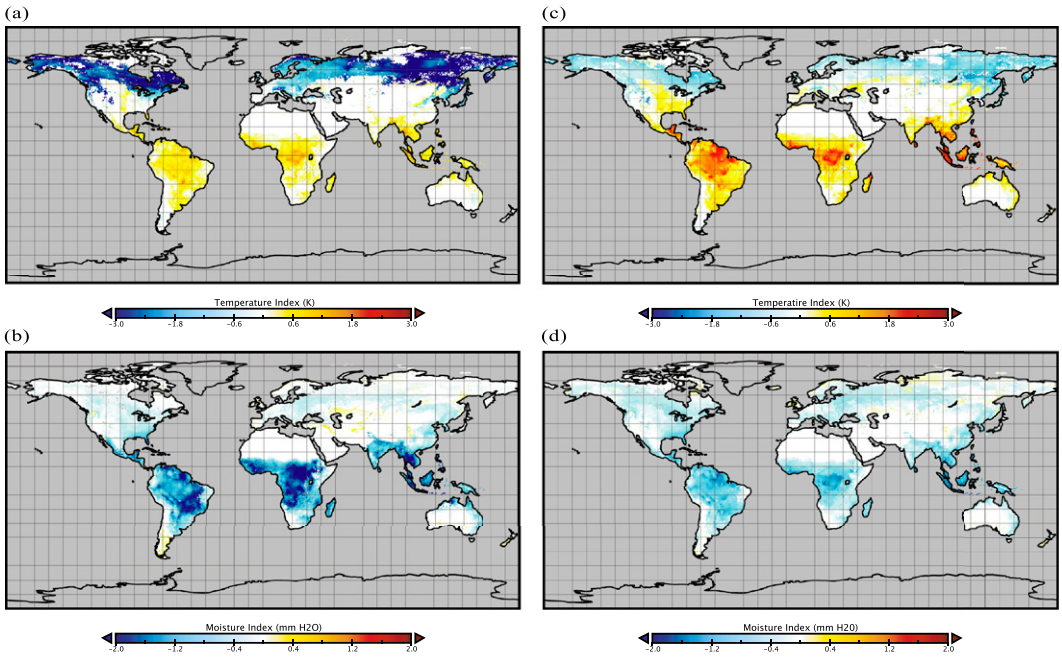

Figure 7. Biogeophysical regulation indices for (a),(c) heat and (b),(d) moisture using (a),(b) PegBL and (c),(d) the simple box boundary layer procedure described in WE10. These indices estimate the potential effect of land-cover change on local boundary layer climate modulated by advected moisture and energy. The largest differences were found in the boreal forest for temperature and the tropics for moisture. In these regions, PegBL's more robust representation of the boundary layer had a significant influence on the biogeophysical regulation of heat and moisture. This can be primarily attributed to PegBL's ability to allow for boundary layer height adjustment in response to changing surface fluxes associated with land-cover change.

forests and boreal forest strongly regulating air temperature relative to advective influences and the tropics having the strongest relative influence on local ABL moisture (Figure 7). However, we found that the tropical biogeophysical influence on moisture and the boreal biogeophysical influence on air temperature to be approximately 2 times that of WE10 because of boundary layer adjustment. This is more in line with conclusions found in previous work on the boreal forest using full GCMs and highlights a strength of this approach (Bonan et al. 1992; Snyder et al. 2004). Additionally, our approach allowed for potential estimation of seasonal variability in the soil–vegetation–boundary layer system and the impact of the daily variation in boundary layer dynamics, which was not possible using WE10's fixed annual average z_i. Alternate devegetation simulations with z_i fixed at potential vegetation levels reinforced the importance of the coevolution of z_i with land-use change, revealing that fixing z_i negates nearly 75% of the cooling associated with land-cover change in the boreal forest and 30% of the tropical drying (Figure 8).

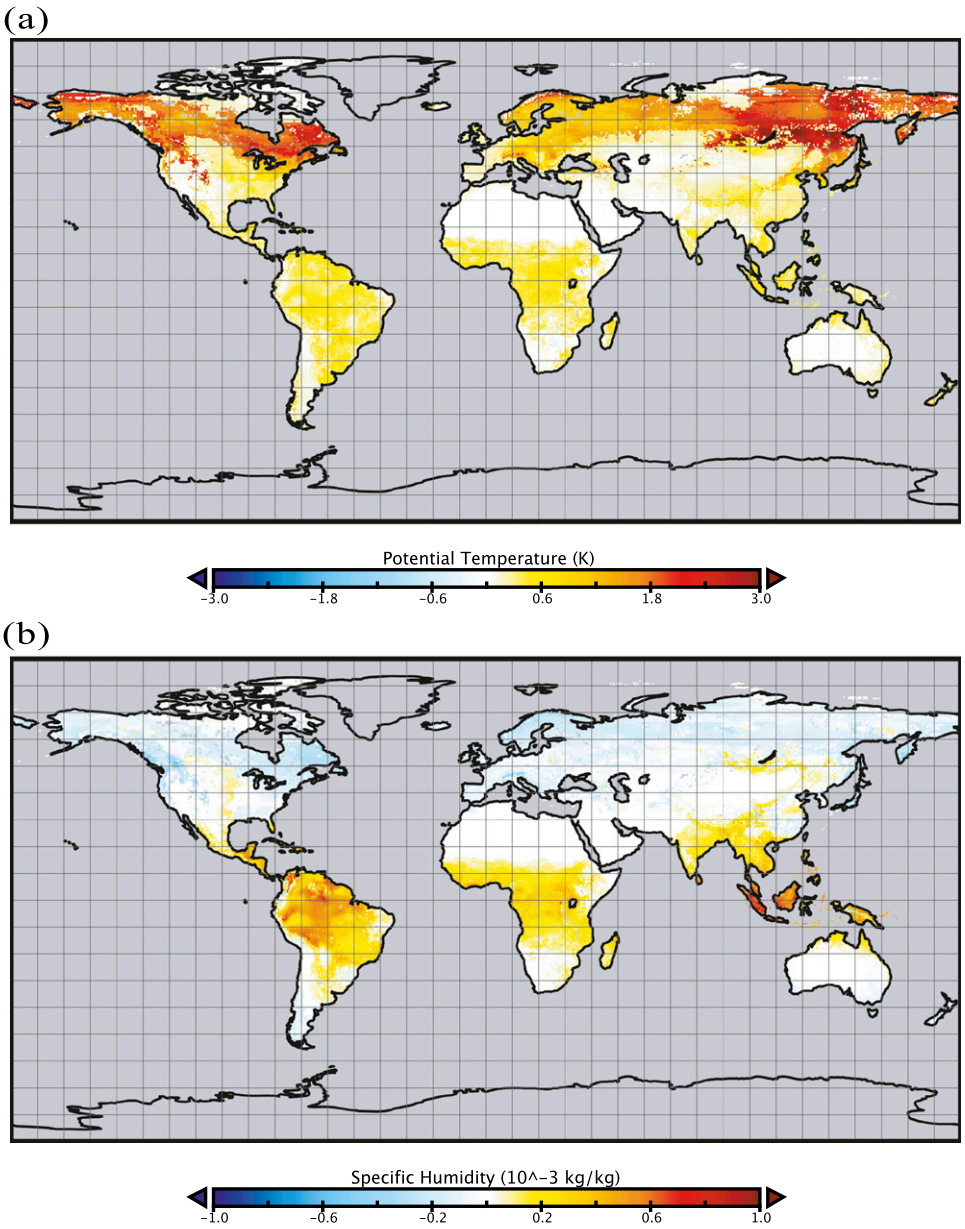

Figure 8. The annual-mean impact of boundary layer height adjustment on (a) ABL potential temperature $\Delta\theta_{bl}$ and (b) ABL specific humidity ΔQ_{bl} for global devegetation scenarios. Here $\Delta\theta_{bl} = \theta_{set} - \theta_{adj}$ and $\Delta Q_{bl} = Q_{set} - Q_{bl}$ with the subscript "adj" denoting θ or Q from a global devegetation simulation where the boundary layer height is allowed to adjust to surface fluxes and the subscript "set" denoting θ or Q from a global devegetation simulation where the boundary layer height is forced to remain at potential vegetation levels. When the boundary layer height is forced to potential vegetation levels, θ (Q) is much larger (smaller) in the northern boreal forests because of artificially increased entrainment of the free atmosphere. Smaller increases in θ and Q are found elsewhere because of a combination of surface sensible and latent heat fluxes to the boundary layer being distributed over smaller air volumes and changes in entrainment.

5. Conclusions

This study presents a simple approach for modeling the biogeophysical impact of land-use/land-cover change scenarios on surface fluxes and the ABL and the near-surface climate. Using input from CRU climatological data, we developed a simple model of the land surface and ABL and have shown that the model can accurately represent the magnitude and daily trends of surface and ABL variables for a variety of biomes with limited inputs. However, care should be taken when comparing results to observations that do not typically represent climatological means because natural variations can have large impacts on energy and moisture budgets. The additional implication of this is that PegBL has limited applicability in regions of high variability where monthly climatological values of physical fields may not be representative of observed values. There are also other limits to the applicability of the model in certain situations given its assumptions. In particular, the model has limited applicability in regions where the night and day heat storage is significantly asymmetric. Finally, in regions of large persistent atmospheric and surface gradients, such as land–sea boundaries, the accuracy of the boundary layer component of the model in its current form is limited, because unaccounted advection of energy and moisture may become a dominant forcing on the atmospheric boundary layer.

Additionally, for vegetation replacement scenarios, PegBL reproduces the gross impacts found by earlier work (Table 5) but with significantly decreased computational time and input requirements. We found that the largest biogeophysical influences on the ABL are located in the boreal and tropical regions. In these regions, it appears the local climatological influence of vegetation on regulating the near-surface atmosphere is significantly larger than climatological influences of advected energy and moisture. However, in regions dominated by nonforested vegetation such as grasslands or savannas, the impact of vegetation removal is reduced, and advection may have a comparable influence. One aspect of land-cover change that we did not consider in this study was the development of urban landscapes in place of natural landscapes. In this case, the biogeophysical impact of replacing natural vegetation with urban landscapes may meet or exceed the vegetation removal scenario we considered here, particularly nonforested regions, and would be a useful case for future studies. We should note that this general framework described here is not specific to one particular land model. Any model (e.g., a crop model) that can produce a reasonable estimate of daily surface energy balance could be used to replace or augment PegBL. However, our evaluation shows that caution is needed to ensure that the energy balance does not violate assumptions about typical diurnal patterns and energy balance closure.

Our approach is limited by its reliance on climatological datasets and the absence of full ocean and atmospheric circulation models. Thus, this work is not intended to replace GCMs or high-resolution mesoscale and LES models. However, PegBL does offer complementary advantages, including reduced computational cost, fewer unknown parameters, a high-resolution representation of the land surface, and a framework for modeling realistic global crop patterns. The approach presented here can be used to quickly assess the effects of land-cover change on major processes that shape local and regional climate without the computation expertise required for more complex approaches. There are many potential

applications, including estimating the climatic effects of the following: expanding croplands in tropical forests; changes in forest distribution in the boreal regional resulting from loss of forest through insect outbreaks and fire; forest expansion in the boreal region resulting from warming trends; and management practices in forested and agricultural landscapes. This combination of advantages should allow interdisciplinary researchers opportunities to estimate impacts of land-cover change from a large variety of global land-use scenarios, a task that is difficult to accomplish with existing models.

Acknowledgments. We thank the contributions of two anonymous reviewers for their helpful comments to improve this work. We would also like to thank C. Barford and W. Sacks for their contributions to development of PEGASUS, M. Sternitzky for her assistance with figure illustrations, and E. Bagley for her helpful comments on early drafts of this manuscript. Also thanks to the Climate Research Unit for providing easily accessible high-resolution data from their website (http://www.cru.uea.ac.uk/cru/data/) and the NOAA/ESRL/Physical Science Division for providing climatological reanalysis (at http://www.esrl.noaa.gov/psd/). This work was accomplished through financial support from the National Science Foundation.

References

Anderson, R. G., and Coauthors, 2010: Biophysical considerations in forestry for climate protection. *Front. Ecol. Environ,* **9,** 174–182.

Bakwin, P., P. P. Tans, D. F. Hurst, and C. Zhao, 1998: Measurements of carbon dioxide on very tall towers: Results of the NOAA/CMDL program. *Tellus,* **50B,** 401–415.

Bala, G., K. Caldeira, M. Wickett, T. J. Phillips, D. B. Lobell, C. Delire, and A. Mirin, 2007: Combined climate and carbon-cycle effects of large-scale deforestation. *Proc. Natl. Acad. Sci. USA,* **104,** 6550–6555.

Baldocchi, D., C. Vogel, and B. Hall, 1997: Seasonal variation of energy and water vapor exchange rates above and below a boreal jack pine forest canopy. *J. Geophys. Res.,* **102,** 28 939–28 951.

——, F. M. Kelliher, T. A. Black, and P. Jarvis, 2008: Climate and vegetation controls on boreal zone energy exchange. *Global Change Biol.,* **6,** 69–83.

Barr, A. G., and A. K. Betts, 1997: Radiosonde boundary layer budgets above a boreal forest. *J. Geophys. Res.,* **102,** 29 205–29 212.

Batjes, N., 2006: ISRIC-WISE derived soil properties on a 5 by 5 arc-minutes global grid (version 1.0). ISRIC World Soil Information Rep., 54 pp. [Available online at http://www.isric.org/isric/webdocs/docs/ISRIC_Report_2006_02.pdf.]

Berger, B., K. J. Davis, C. Yi, P. S. Bakwin, and C. L. Zhao, 2001: Long-term carbon dioxide fluxes from a very tall tower in a northern forest: Flux measurement methodology. *J. Atmos. Oceanic Technol.,* **18,** 529–542.

Betts, A. K., and J. Ball, 1998: FIFE surface climate and site-average dataset 1987–89. *J. Atmos. Sci.,* **55,** 1091–1108.

Betts, R., 2000: Offset of the potential carbon sink from boreal forestation by decreases in surface albedo. *Nature,* **408,** 187–190.

Bhumralkar, C., 1975: Numerical experiments on the computation of ground surface temperature in an atmospheric general circulation model. *J. Appl. Meteor.,* **14,** 1246–1258.

Blackadar, A., 1976: Modeling the nocturnal boundary-layer. *Bull. Amer. Meteor. Soc.,* **57,** 631–631.

Bonan, G. B., 1997: Effects of land use on the climate of the United States. *Climatic Change,* **37,** 449–486.

——, D. Pollard, and S. L. Thompson, 1992: Effects of boreal forest vegetation on global climate. *Nature,* **359,** 716–718.

Bounoua, L., R. DeFries, G. J. Collatz, P. Sellers, and H. Khan, 2002: Effects of land cover conversion on surface climate. *Climatic Change,* **52,** 29–64.

Brutsaert, W., 1975: On a derivable formula for long-wave radiation from clear skies. *Water Resour. Res.,* **11,** 742–744.

Campbell, G., and J. Norman, 2000: *An Introduction to Environmental Biophysics*. Springer-Verlag, 286 pp.

Chapin, F. S., III, J. T. Randerson, A. D. McGuire, and J. A. Foley, 2008: Changing feedbacks in the climate-biosphere system. *Front. Ecol. Environ.,* **6,** 313–320.

Choudhury, B., and N. Digirolamo, 1998: A biophysical process-based estimate of global land surface evaporation using satellite and ancillary data I. Model description and comparison with observations. *J. Hydrol.,* **205,** 164–185.

Clausen, M., and Coauthors, 2002: Earth system models of intermediate complexity: Closing the gap in the spectrum of climate models. *Climate Dyn.,* **18,** 579–586.

Costanza, R., and Coauthors, 1997: The value of the world's ecosystem services and natural capital. *Nature,* **387,** 253–260.

Culf, A. D., J. L. Esteves, A. O. Marques Filho, and H. R. da Rocha, 1996: Radiation, temperature and humidity over forest and pastures in Amazonia. *Amazonian Deforestation and Climate,* J. Gash et al. Eds., John Wiley & Sons, 175–192.

Davin, E., and N. de Noblet-Ducoudré, 2010: Climatic impact of global-scale deforestation: Radiative versus nonradiative processes. *J. Climate,* **23,** 97–112.

Davis, K. J., P. S. Bakwin, C. Yi, B. W. Berger, C. Zhao, R. M. Teclaw, and J. G. Isebrands, 2003: The annual cycles of CO_2 and H_2O exchange over a northern mixed forest as observed from a very tall tower. *Global Change Biol.,* **9,** 1278–1293.

Denning, A., N. Zhang, C. Yi, M. Branson, K. Davis, J. Kleist, and P. Bakwin, 2008: Evaluation of modeled atmospheric boundary layer depth at the WLEF tower. *Agric. For. Meteor.,* **148,** 206–215.

Deryng, D., W. J. Sacks, C. C. Barford, and N. Ramankutty, 2010: Simulating the effects of climate and agricultural management practices on global crop yield. *Global Biogeochem. Cycles,* **25,** GB2006, doi:10.1029/2009GB003765.

Desai, A. R., B. R. Helliker, P. R. Moorcroft, A. E. Andrews, and J. A. Berry, 2010: Climatic controls of interannual variability in regional carbon fluxes from top-down and bottom-up perspectives. *J. Geophys. Res.,* **115,** G02011, doi:10.1029/2009JG001122.

Dolman, A., A. D. Culf, and P. Bessemoulin, 1997: Observations of boundary layer development during the HAPEX-Sahel intensive observation period. *J. Hydrol.,* **188,** 998–1016.

Eugster, W., and Coauthors, 2000: Land–atmosphere energy exchange in Arctic tundra and boreal forest: Available data and feedbacks to climate. *Global Change Biol.,* **6,** 84–115.

Feddema, J., K. W. Oleson, G. B. Bonan, L. O. Mearns, L. E. Buja, G. A. Meehl, and W. M. Washington, 2005: The importance of land-cover change in simulating future climates. *Science,* **310,** 1674–1678.

Fisch, G., J. Tota, L. A. T. Machado, M. A. F. Silva Dias, R. F. da F. Lyra, C. A. Nobre, A. J. Dolman, and J. H. C. Gash, 2004: The convective boundary layer over pasture and forest in Amazonia. *Theor. Appl. Climatol.,* **78,** 47–59.

Foley, J. A., M. H. Costa, C. Delire, N. Ramankutty, and P. Snyder, 2003: Green surprise? How terrestrial ecosystems could affect Earth's climate. *Front. Ecol. Environ,* **1,** 38–44.

——, and Coauthors, 2005: Global consequences of land use. *Science,* **309,** 570–574.

——, and Coauthors, 2007: Amazonia revealed: Forest degradation and loss of ecosystem goods and services in the Amazon basin. *Front. Ecol. Environ,* **5,** 25–32.

Friedl, M., 2002: Forward and inverse modeling of land surface energy balance using surface temperature measurements. *Remote Sens. Environ.,* **79,** 344–354.

Friend, A., 1998: Parameterisation of a global daily weather generator for terrestrial ecosystem modelling. *Ecol. Modell.,* **109,** 121–140.

Gash, J., and C. Nobre, 1997: Climatic effects of Amazonian deforestation: Some results from ABRACOS. *Bull. Amer. Meteor. Soc.,* **78,** 823–830.

Gerten, D., S. Schaphoff, U. Haberlandt, W. Lucht, and S. Sitch, 2004: Terrestrial vegetation and water balance—Hydrological evaluation of a dynamic global vegetation model. *J. Hydrol.,* **286,** 249–270.

Goutorbe, J.-P., and Coauthors, 1994: HAPEX-Sahel: A large-scale study of land-atmosphere interactions in the semi-arid tropics. *Ann. Geophys.,* **12,** 53–64.

Hartmann, D., 1994: *Global Physical Climatology.* Academic Press, 411 pp.

Kalnay, E., and Coauthors, 1996: The NCEP/NCAR 40-Year Reanalysis Project. *Bull. Amer. Meteor. Soc.,* **77,** 437–471.

Kim, C., and D. Entekhabi, 1998: Feedbacks in the land-surface and mixed-layer energy budgets. *Bound.-Layer Meteor.,* **88,** 1–21.

Kustas, W., and C. Daughtry, 1990: Estimation of the soil heat flux/net radiation ratio from spectral data. *Agric. For. Meteor.,* **49,** 205–223.

Legates, D. R., and T. A. Bogart, 2009: Estimating the proportion of monthly precipitation that falls in solid form. *J. Hydrometeor.,* **10,** 1299–1306.

Liebethal, C., and T. Foken, 2007: Evaluation of six parameterization approaches for the ground heat flux. *Theor. Appl. Climatol.,* **88,** 43–56.

Linacre, E., 1968: Estimating the net-radiation flux. *Agric. Meteor.,* **5,** 49–63.

Liu, H., J. T. Randerson, J. Lindfors, and F. S. Chapin III, 2005: Changes in the surface energy budget after fire in boreal ecosystems of interior Alaska: An annual perspective. *J. Geophys. Res.,* **110,** D13101, doi:10.1029/2004JD005158.

Margulis, S., and D. Entekhabi, 2001: A coupled land surface–boundary layer model and its adjoint. *J. Hydrometeor.,* **2,** 274–296.

Meir, P., P. Cox, and J. Grace, 2006: The influence of terrestrial ecosystems on climate. *Trends Ecol. Evol.,* **21,** 256–260.

Millennium Ecosystem Assessment, 2005: *Ecosystems and Human Well-Being Synthesis*. Island Press, 155 pp.

Mitchell, T., and P. Jones, 2005: An improved method of constructing a database of monthly climate observations and associated high-resolution grids. *Int. J. Climatol.,* **25,** 693–712.

Moeng, C., 1984: A large-eddy-simulation model for the study of planetary boundary-layer turbulence. *J. Atmos. Sci.,* **41,** 2052–2062.

Monteith, J., 1995: Accommodation between transpiring vegetation and the convective boundary layer. *J. Hydrol.,* **166,** 251–263.

New, M., D. Lister, M. Hulme, and I. Makin, 2002: A high-resolution data set of surface climate over global land areas. *Climate Res.,* **21,** 1–25.

Oke, T., 1987: *Boundary Layer Climates*. Routledge, 464 pp.

Prentice, C. I., M. T. Sykes, and W. Cramer, 1993: A simulation-model for the transient effects of climate change on forest landscapes. *Ecol. Modell.,* **65,** 51–70.

Ramankutty, N., and J. Foley, 1999: Estimating historical changes in global land cover: Croplands from 1700 to 1992. *Global Biogeochem. Cycles,* **13,** 997–1027.

——, A. T. Evan, C. Monfreda, and J. A. Foley, 2008: Farming the planet: 1. Geographic distribution of global agricultural lands in the year 2000. *Global Biogeochem. Cycles,* **22,** GB1003, doi:10.1029/2007GB002952.

Randall, D. S., and M. Branson, 1998: Representation of clear and cloudy boundary layers in climate models. *Clear and Cloudy Boundary Layers,* A. A. M. Holtslag and P. G. Duynkerke, Eds., Royal Netherlands Academy of Arts and Science, 305–322.

Santanello, J., Jr., and M. Friedl, 2003: Diurnal covariation in soil heat flux and net radiation. *J. Appl. Meteor.,* **42,** 851–862.

Sellers, P. J., F. G. Hall, G. Asrar, D. E. Strebel, and R. E. Murphy, 1988: The First ISLSCP Field Experiment (FIFE). *Bull. Amer. Meteor. Soc.,* **69,** 22–27.

——, and Coauthors, 1997: BOREAS in 1997: Experiment overview, scientific results, and future directions. *J. Geophys. Res.,* **102,** 28 731–28 769.

Shukla, J., C. Nobre, and P. Sellers, 1990: Amazon deforestation and climate change. *Science,* **247,** 1322–1325.

Snyder, P., C. Delire, and J. A. Foley, 2004: Evaluating the influence of different vegetation biomes on the global climate. *Climate Dyn.,* **23,** 279–302.

Stull, R., 1988: *An Introduction to Boundary Layer Meteorology.* Atmospheric Sciences Library, 680 pp.

Tennekes, H., 1973: A model for the dynamics of the inversion above a convective boundary layer. *J. Atmos. Sci.,* **30,** 558–567.

Troen, I., and L. Mahrt, 1986: A simple model of the atmospheric boundary layer; Sensitivity to surface evaporation. *Bound.-Layer Meteor.,* **37,** 129–148.

von Randow, C., and Coauthors, 2004: Comparative measurements and seasonal variations in energy and carbon exchange over forest and pasture in south west Amazonia. *Theor. Appl. Climatol.,* **78,** 5–26.

West, P. C., G. T. Narisma, C. C. Barford, C. J. Kucharik, and J. A. Foley, 2010: An alternative approach for quantifying climate regulation by ecosystems. *Front. Ecol. Environ.,* **9,** 126–133.

Wilczak, J., 1999: BOREAS AFM-06 boundary layer height data. Oak Ridge National Laboratory Distributed Active Archive Center Dataset. [Available online at http://daac.ornl.gov/cgi-bin/dsviewer.pl?ds_id=240.]

Yi, C., K. J. Davis, P. S. Bakwin, A. S. Denning, N. Zhang, A. Desai, J. C. Lin, and C. Gerbig, 2004: Observed covariance between ecosystem carbon exchange and atmospheric boundary layer dynamics at a site in northern Wisconsin. *J. Geophys. Res.,* **109,** D08302, doi:10.1029/2003JD004164.

Zhang, H., A. Henderson-Sellers, and K. McGuffie, 1996: Impacts of tropical deforestation. Part I: Process analysis of local climatic change. *J. Climate,* **9,** 1497–1517.

Zilitinkevich, S., and A. Baklanov, 2002: Calculation of the height of the stable boundary layer in practical applications. *Bound.-Layer Meteor.,* **105,** 389–409.